AGU PUBLICATIONS

Water Resources Research

RESEARCH ARTICLE
10.1002/2014WR015587

Key Points:
- Random field approach is utilized for assessing elevation and depth variability
- Bed elevation standard deviation and depth skew effectiveness for predicting *f*
- Skew and kurtosis are valuable for quantifying the spectrum of channel types

Correspondence to:
S. E. Yochum,
steven.yochum@usda.gov

Citation:
Yochum, S. E., B. P. Bledsoe, E. Wohl, and G. C. L. David (2014), Spatial characterization of roughness elements in high-gradient channels of the Fraser Experimental Forest, Colorado, USA, *Water Resour. Res.*, *50*, doi:10.1002/2014WR015587.

Received 17 MAR 2014
Accepted 25 JUN 2014
Accepted article online 30 JUN 2014

Spatial characterization of roughness elements in high-gradient channels of the Fraser Experimental Forest, Colorado, USA

Steven E. Yochum[1,2], Brian P. Bledsoe[1], Ellen Wohl[3], and Gabrielle C. L. David[3,4]

[1]Department of Civil and Environmental Engineering, Colorado State University, Fort Collins, Colorado, USA, [2]Now at USDA Natural Resources Conservation Service, Fort Collins, Colorado, USA, [3]Department of Geosciences, Colorado State University, Fort Collins, Colorado, USA, [4]Now at Department of Earth and Environmental Science, Boston College, Chestnut Hill, Massachusetts, USA

Abstract We collected high-resolution LiDAR-based spatial and reach-average flow resistance data at a range of flows in headwater stream channels of the Fraser Experimental Forest, Colorado, USA. Using these data, we implemented a random field approach for assessing the variability of detrended bed elevations and flow depths for both the entire channel width and the thalweg-centered 50% of the channel width (to exclude bank effects). The spatial characteristics of these channels, due to bedforms, large clasts and instream wood, were compared with Darcy-Weisbach *f* and stream type through the use of the first four probability density function moments (mean, variance, skewness, kurtosis). The standard deviation of the bed elevations (σ_z) combined with depth (h), as relative bedform submergence (h/σ_z), was well correlated with *f* ($R^2 = 0.81$) for the 50% of channel width. The explained variance decreased substantially ($R^2 = 0.69$) when accounting for the entire width, indicating lesser contribution of channel edges to flow resistance. The flow depth skew also explained a substantial amount of the variance in *f* ($R^2 = 0.78$). A spectrum of channel types is evident in depth plots of skew versus kurtosis, with channel types ranging from plane bed, transitional, step pool/cascade, to cascade. These results varied when bank effects were included or excluded, although definitive patterns were observed for both analyses. Random field analyses may be valuable for developing tools for predicting flow resistance, as well as for quantifying the spectrum of morphologic change in high-gradient channel types, from plane bed through cascade.

1. Introduction

The spatial characterization of alluvial channels can be valuable for describing geomorphic form, for such applications as roughness and sediment transport prediction as well as stream type descriptions and quantification of biotic habitat. Longitudinal profiles, which are two-dimensional spatial data that are commonly collected in the channel thalweg, have been a standard tool for describing fluvial geomorphology while such tools as Light Detection and Ranging (LiDAR), total stations, acoustic soundings, and survey-grade GPS provide opportunities to describe the three-dimensional form of stream channels through pointclouds and digital elevation models (DEMs). Stream channel form has been assessed using both longitudinal profiles and DEMs through an evaluation of the continuous wavefields, using such tools as the random field approach to assess statistical variability.

The random field approach has long been utilized to evaluate bedform characteristics and dynamics in alluvial channels [*Kennedy*, 1963; *Hino*, 1968; *Nordin*, 1971; *Jain and Kennedy*, 1974; *Furbish*, 1987; *Robert*, 1988; *Clifford et al*., 1992; *Nikora et al*., 1997] using data collected in laboratory and field settings. The random field approach implements continuous spatial stream data, typically treating topographic survey data as a random field of bed elevations and describing these forms using such probability density function moments as the mean, variance, skew, and kurtosis, as well as correlation, spectra, and structure functions [*Aberle et al*., 2010; *Coleman et al*., 2011]. The more recent availability of high-resolution DEMs has allowed the use of the random field approach to spatially characterize bedforms in a more comprehensive way [*Aberle and Nikora*, 2006; *Aberle et al*., 2010; *Coleman et al*., 2011]. These studies have commonly focused on lower-gradient sand-bed channels, with plane bed, ripple, dune and antidune bedforms, although numerous analyses have also been performed on gravel-bed streams [*Furbish*, 1987; *Robert*, 1988; *Clifford et al*., 1992; *Nikora et al*.,

1998; *Aberle and Smart*, 2003; *Nikora and Walsh*, 2004; *Aberle and Nikora*, 2006; *Coleman et al*., 2011], while limited work has been performed in higher-gradient channels [*Aberle and Smart*, 2003; *Trevisani et al*., 2010].

A substantial amount of recent field-based work has focused on flow resistance in high gradient channels. For example, the impact of grain size and relative grain submergence, boulder clustering, stream type, and instream wood density on flow resistance has been investigated [*Lee and Ferguson*, 2002; *Ferguson*, 2007; *Reid and Hickin*, 2008; *Wohl and Merritt*, 2008; *David et al*., 2010a; *David et al*., 2011; *Nitsche et al*., 2012]. Additionally, bedforms have been assessed for their contributions to flow resistance and usefulness for resistance and flow velocity prediction [*Aberle and Smart*, 2003; *Yochum et al*., 2012; *Nitsche et al*., 2012]. These works have typically focused on two-dimensional spatial data sets, such as longitudinal profiles, and specific feature surveys (boulder or wood presence, concentration, size), rather than three-dimensional channel forms. This is understandable considering the substantial challenges associated with measuring the entire form of stream channels in the field, in mountainous settings.

A data set collected in high-gradient stream channels of the Fraser Experimental Forest, Colorado, USA, with measured average reach velocity and flow resistance measurements combined with LiDAR and total station measurements of bedform and other flow resistance structures, provides an opportunity to explore three-dimensional spatial relationships in cascade, step pool and plane bed stream channels and illuminate random field variables helpful for quantifying bedforms and their contribution to flow resistance. While a number of previous works based on the 15 stream reaches of the Fraser data set have been published [*David et al*., 2010a, 2010b, 2011, *Yochum et al*., 2012], this is the first article to explore the three-dimensional forms as described by the LiDAR data set. To that end, the goal of this paper is to evaluate the application of the mean, variance, skew, and kurtosis statistical moments for describing bedform characteristics in these high-gradient channels and relating the descriptors to flow resistance and channel type. Grouped sets of these spatial variables describing reach-average detrended DEMs and depth variability are compared to flow resistance. Bank affects are explored by both including and excluding data collected in the vicinity of the channel margins. Channel types are also compared to *Sk-Ku* plots, to assess the capability of such a method for quantifying a spectrum of channel types, from plane bed though cascade.

2. Methods

We collected spatial information and average reach velocity data in 15 high-gradient channels of the U.S. Forest Service (USFS) Fraser Experimental Forest, CO, USA, in East Saint Louis (ESL) Creek and Fool Creek (FC). These are snowmelt-dominated streams, with catchment sizes varying from 0.69 to 8.5 km^2. Data were collected on four cascades, nine step-pools, one transitional, and one plane-bed stream reaches, with slopes ranging from 1.5 to 20%. Instream wood was present in all reaches, both within steps and dispersed throughout the reaches. Large clasts anchored instream wood, increasing step heights, bed variability and flow resistance. Reaches were initiated and terminated at similar bedform points and had consistent morphology, depth variability, and wood loading throughout. The reach breaks were verified through inspection of longitudinal profiles. Four of the 15 reaches are illustrated in Figure 1; additional photographs are available [*Yochum*, 2010; *Yochum and Bledsoe*, 2010; *Yochum et al*. 2014].

Average reach velocity was measured using a Rhodamine WT tracer, for discharges ranging from low to approximately bankfull. Discharge was measured by the USFS using sharp-crested weirs. Spatial data were collected using terrestrial LiDAR scanning for above low-flow channel features, with longitudinal profiles and gridded point data collected using a total station for below-water features, providing a high-resolution geometric representation of the stream reaches at each specific flow. The velocity data were used in combination with the spatial data to compute the Darcy-Weisbach *f*. A summary of the field data collection and computational methodologies are provided below. For additional details on these techniques, see *Yochum* [2010], *David et al*. [2010a], and *Yochum et al*. [2012].

2.1. Velocity and Flow Resistance

Average reach velocities were computed as the thalweg flow path length divided by the travel time. The travel time was measured using Rhodamine WT dye, with replicates of four to five injections. Measurements were made at a 1 s time step using two synchronized fluorometers mounted to rebar in the thalweg at the reach limits. Travel time was computed using a spatial harmonic mean, which can be the most appropriate

Figure 1. Typical reach conditions, during low flow. Average bankfull width: 1.0 to 3.0 m.

method under steady flow conditions [*Walden*, 2004; *Zimmermann*, 2010]. Additional details of the methodology are provided in *Yochum* [2010]. To address data noise due to sunlight and aeration, a single-pass three-point median smoothing methodology was applied to the tracer data [*Tukey*, 1974]. Median smoothing tends to preserve sharp signal edges while filtering out impulses [*Gallagher and Wise*, 1981; *Ataman et al.*, 1981].

The Darcy-Weisbach equation is:

$$V = \sqrt{\frac{8gRS_f}{f}} \tag{1}$$

where V is the average reach velocity (m/s); f is the friction factor; S_f is the friction slope (m/m); g is the acceleration due to gravity; R, the hydraulic radius, is computed as A/P_w; A is the cross-sectional area (m^2); and P_w

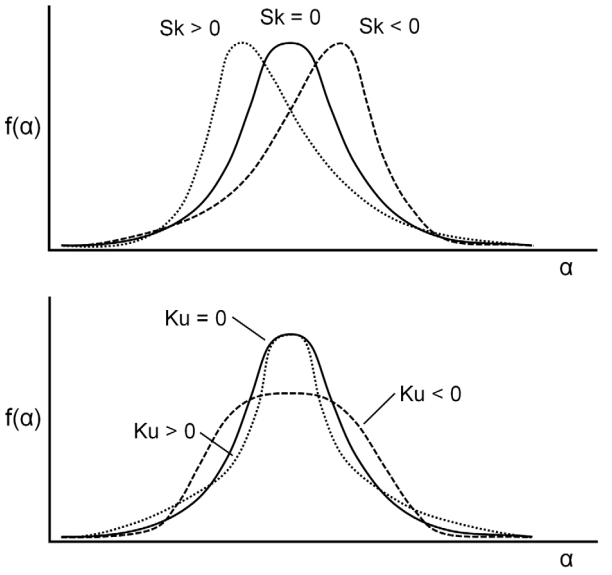

Figure 2. Probability density function schematic, illustrating skew (*Sk*) and kurtosis (*Ku*).

is the wetted perimeter (m). All of the terms are reach-averaged values, hence providing average flow resistance in each reach at each flow stage.

2.2. Spatial Surveying and Processing

Spatial data were collected with a terrestrial LiDAR scanner (Leica HDS Scanstation) for features above the low flow water surface, at 1 to 5 cm scale. Each of the reaches was scanned from multiple directions to minimize shadow. For below-water features, gridded points and longitudinal profile points were collected with a total station, at a 5 to 30 cm scale (depending upon bed variability). The fifteen reach lengths varied from 6.2 to 35 m, with flow widths from 0.7 to 4.0 m. From the LiDAR scans and additional total station data, cross sections were developed at an interval of 0.75 to 1.50 m over the 6–35 m reach lengths, for a total of nine to 27 sections for each reach. Averages of these cross-sectional data were used to compute the *f* values.

The processing of the spatial data was performed in Leica Cyclone (version 6.0) and ArcGIS (version 9.3). In these heavily vegetated reaches, the initial LiDAR pointclouds had a substantial amount of nonflow-impacting vegetation also picked up by the scans. This geometric noise was manually removed. After this step, for the nonlow flow resistance measurements, the following process was followed to extract the spatial data utilized in this analysis, for each of the 44 flow resistance measurements. From longitudinal surveys of the water surface, at the thalweg, and left and right channel edges, triangular irregular network (TIN) mesh models of the water surface were created, from which 5cm resolution DEMs were created. Using the resulting water surface extent (which varies for each measurement), the bed point clouds were cleaned to remove all points outside the flow volume, hence providing a spatial field that includes bedform features, large clasts, and instream wood. Breaklines were then created, to provide the most appropriate representation of bedform. Using the pointclouds and breaklines, a TIN and 5cm DEM were created. From these two sets of DEMs, two different spatial data sets were developed: a depth variability data set, computed by simply subtracting the bed DEM from the water surface TIN, and a detrended bed elevation data set. This detrended data set was computed by setting a reference plane along the channel thalweg, with the origin at the upstream terminus of the thalweg longitudinal profile, x axis aligned with the longitudinal profile, y axis as the transverse dimension, and z axis set with an origin along the regression of the longitudinal profile. The results indicate that this method reasonably detrended the data set, though the absolute effectiveness of the method for eliminating all of the slope affects is unknown. Finally, to assess bank affects, the center 50% of the reach was extracted using an analysis mask centered about the thalweg. This 50% was selected in response to field observations (at about bankfull flow) that the center 50% of the channel width was substantially more effective for conveyance. For additional information on the methods utilized for extracting this information, see *Yochum* [2010].

2.3. Statistical Analyses

Probability density function moments can be an effective method for describing and interpreting bed morphology; in this paper, both detrended bed elevations and flow depths were assessed. Assuming a homogeneous and ergodic field [*Aberle et al*., 2010, *Coleman et al*., 2011], with ergodic referring to a situation where, generally speaking, the field has the same behavior when averaged over both time and space, the first four moments describing a surface spatial distribution were computed as:

$$\text{mean} = \mu = \frac{1}{n}\sum_{i=1}^{n} \alpha_i$$

$$\text{variance} = \sigma^2 = \frac{1}{n}\sum_{i=1}^{n} (\alpha_i - \mu)^2$$

$$\text{skewness} = Sk = \frac{n}{(n-1)(n-2)}\sum_{i=1}^{n} \left(\frac{\alpha_i - \mu}{\sigma}\right)^3$$

$$\text{kurtosis} = Ku = \left[\frac{n(n+1)}{(n-1)(n-2)(n-3)}\left(\frac{\alpha_i - \mu}{\sigma}\right)^4\right] - \frac{3(n-1)^2}{(n-2)(n-3)}$$

where α is the individual spatial measurement, and σ is the standard deviation.

Skew and kurtosis variability are illustrated in Figure 2. A positive skew (*Sk*) indicates a preponderance of lower (detrended) elevation or depth values in a population of reach measurements, with higher, outlying values present, while a negative skew indicates a preponderance of higher magnitude measurements, with lower, outlying values present. A negative kurtosis (*Ku*) indicates more consistent (detrended) elevation or depth measurements (variance is due to moderately sized deviations), while a positive kurtosis indicates less consistent measurements (variance is more the result of extreme deviations, i.e., heavy tails). Due to bank effects, the inclusion of the channel edges in these small channels may violate the assumption of homogeneity; computations were performed for both the entire channel width and the center 50% of the channel width and the results compared.

Simple linear and multivariate regressions were performed on the assembled data set, using R (version 2.1.2). Where appropriate, natural logarithmic transformations were applied, which provided good adherence to the regression assumptions of linearity, homoscedasticity, and independent and normally distributed residuals.

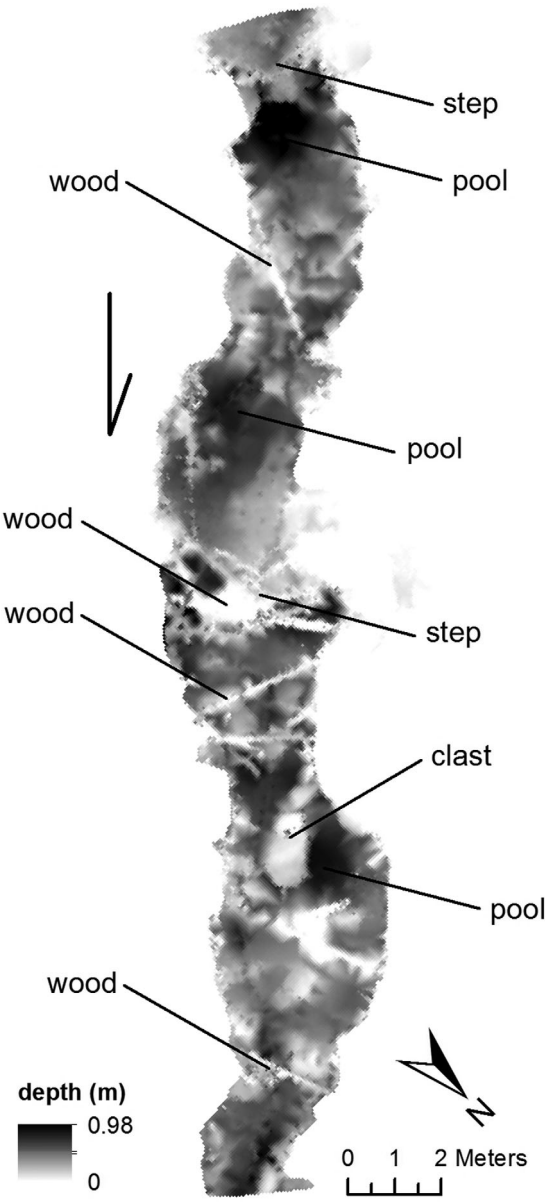

Figure 3. Depth variability for bankfull flow, reach ESL-1. Pixel size is 5 cm, with 32,300 points.

3. Results

Forty four sets of flow resistance, detrended DEM, and depth variability were computed. These data sets were quantified using probability density function moments, and compared by reach type. Each of the 44 measurements on the 15 reaches was unique,

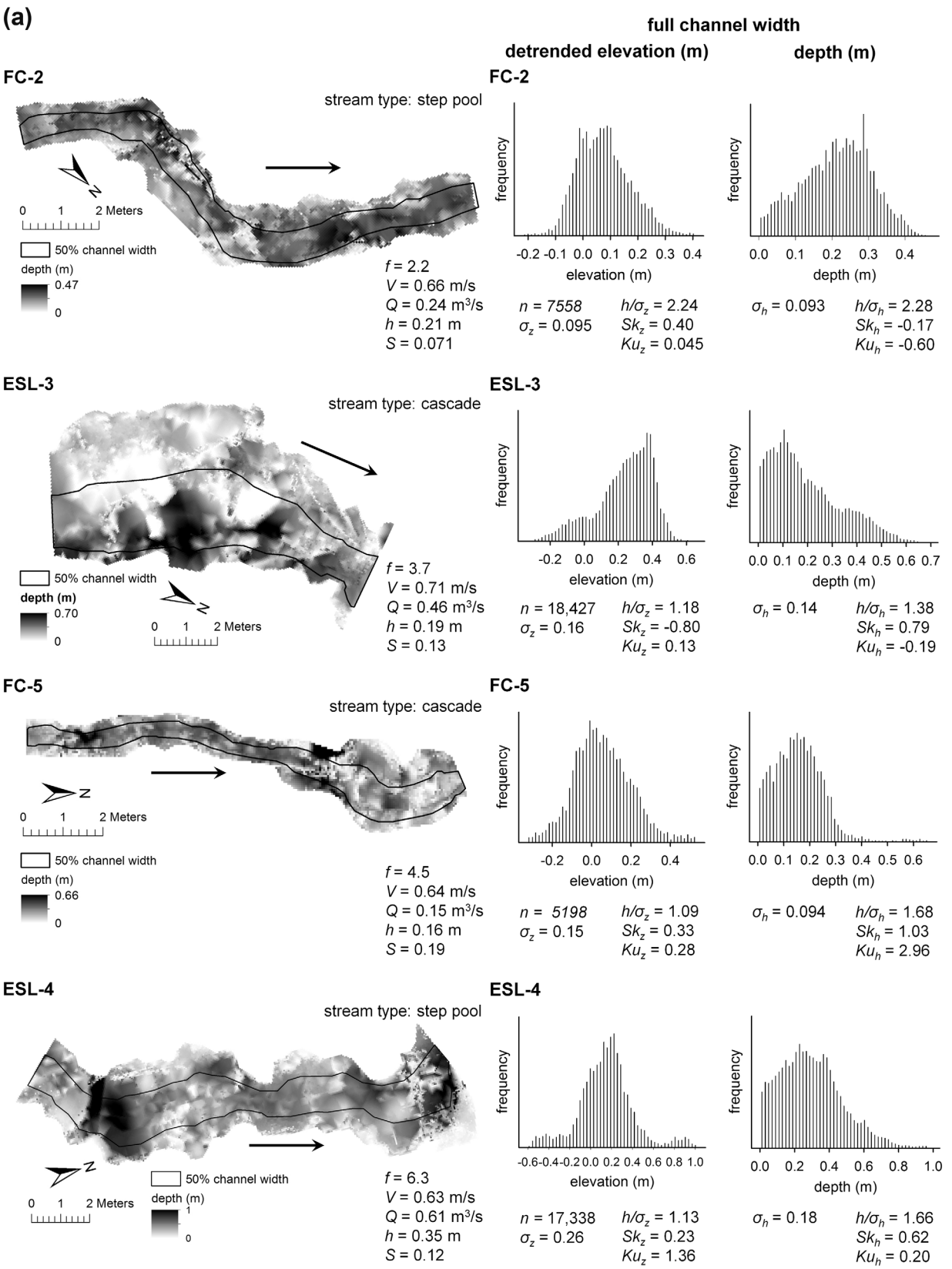

Figure 4. (a) Example bed variability plots and histograms, at about bankfull flow and ordered with increasing flow resistance. See text for symbol definitions. (b) Example bed variability plots and histograms, at about bankfull flow and ordered with increasing flow resistance. See text for symbol definitions.

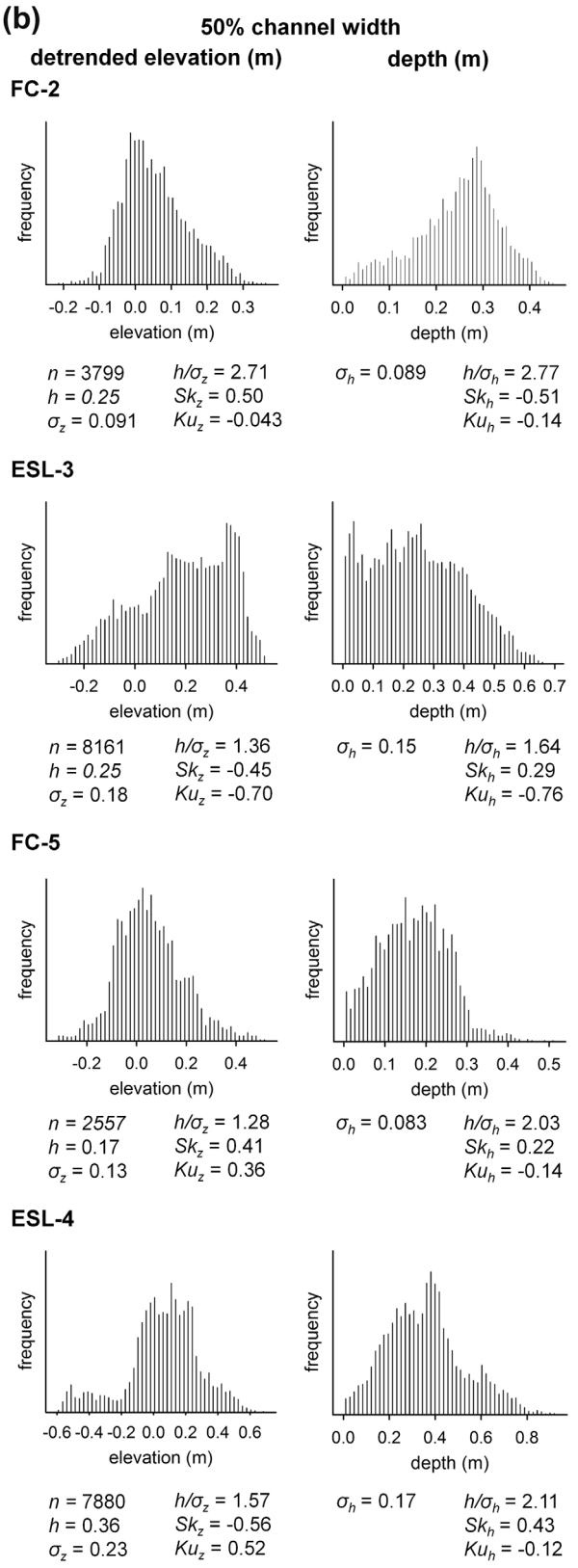

Figure 4. (continued)

reflecting the variability in flow extent and stage by discharge. Depth variability for reach ESL-1 at bankfull flow is illustrated (Figure 3). This image illustrates key flow resistance elements and the spatial resolution. Depth variability is shown, rather than detrended elevation, since flow resistance features are more easily observed in the depth variability plots.

Four example sets of measurements collected at about bankfull flow, spanning a range in channel types, are summarized (Figure 4), with the additional data provided (Appendix A). The figure is ordered (from top to bottom) with increasing flow resistance. Figure 4a provides general reach characteristics, such as measured flow resistance, average reach velocity, average discharge at which the measurement was collected, average depth throughout the field of n points, and friction slope, while also providing histograms and metrics describing the detrended elevation and flow depth fields for the full channel width. These descriptors are the standard deviation, the three-dimensional relative bedform submergence (h/σ) [*Yochum et al.*, 2012], and the skew and kurtosis for both the detrended elevation (subset z) and depth (subset h). Histograms and metrics for the 50% channel width, about the thalweg, are also provided (Figure 4b). The extent of this censored data set is illustrated in the depth variability plots of Figure 4a. The bin count for each histogram is 50.

Plots illustrating the relationship of flow resistance with h/σ, as well as Sk and Ku, for detrended elevation and depth and for both the full and 50% channel widths, are illustrated (Figure 5). The coefficient of determination (R^2) of each relationship is also provided. These fits correspond to power relationships (h/σ, Figures 5a–5d), exponential relationships (Sk_h, Figures 5f and 5h), and linear relationships (Sk_z, Ku). In general, h/σ is highly related to flow resistance, Sk_h is well related to flow resistance while Sk_z is not, and Ku is poorly correlated with flow resistance in these high-gradient channels.

Following work by *Coleman et al.* [2011] in gravel and sand-bed channels, Sk versus Ku plots were developed for these high-gradient

cobble and boulder dominated channels (Figure 6). These *Sk-Ku* planes were computed for the detrended elevation and depth, for both the full and 50% channel widths. The depth *Sk-Ku* field plots indicate a spectrum of channel types across the plane, from plane bed to cascade.

4. Discussion

This LiDAR-derived high-resolution spatial data set of high-gradient channels in the Fraser Experimental Forest, with corresponding measurements of reach-average flow resistance at a range of discharges, provides an opportunity for exploration of three-dimensional measures of geometric variability though a random field analysis. This field analysis includes elevation and depth variability due to bedform induced by instream wood and large clasts, discrete pieces of instream wood, and, in the case of the full channel width analyses, bankform. The characteristics of detrended elevations and depths were investigated and compared to the Darcy-Weisbach *f*. Detrending the elevations was necessary, to exclude variation due to slope. Using longitudinal profiles and the entire data set of 59 measurements, not detrending the data reduced the explained variance for *f* versus h/σ_z from 80 to 58% [*Yochum et al*., 2012].

4.1. Random Field Characteristics and Flow Resistance

Relative bedform submergence (h/σ_z) is inversely proportional to flow resistance in the Fraser stream reaches (Figures 5a–5d). As indicated by correlation, submergence based on σ_z is more effective than σ_h, with exclusion of the outer edges of the channel increasing the prediction accuracy. Using the center 50% of the channel width, h/σ_z explains 81% in the variation in the Darcy-Weisbach *f*. The reduction in explained variance when using the entire channel width indicates that channel edges contribute less to flow resistance than the thalweg area in these channel types, which is a reasonable finding since morphological variation is more vertical than horizontal in steep streams. Additionally, the finding that σ_z is powerful for prediction makes sense, since greater bed elevation variability provides more opportunity for both form and spill flow resistance. Form resistance is caused by secondary currents and eddying from such obstacles as boulders, instream wood, and bank variability. Spill resistance is incurred from a sudden flow deceleration, where rapid flow and impinging jets impact on slow-moving water, resulting in turbulence and hydraulic jumps. In high-gradient channels, spill resistance is typically dominant [*Kaufmann*, 1987; *Curran and Wohl*, 2003; *MacFarlane and Wohl*, 2003; *Wilcox et al*., 2006; *Kaufmann et al*., 2008; *Comiti et al*., 2009; *David et al*., 2011]; the finding that h/σ_z is well correlated with flow resistance supports these findings.

Submergence computed from a thalweg longitudinal profile [*Yochum et al*., 2012] for this data set explains the same amount of variance, with the three-dimensional computations well correlated ($R^2 = 0.85$) with two-dimentional longitudinal profile values. Hence, the Fraser data set indicates that flow resistance prediction using relative bedform submergence computed from the three-dimensional variability provides no advantage to submergence computed from simpler-to-measure longitudinal profiles. This is helpful for prediction and application since longitudinal profiles are simpler to measure. It also illustrates the dominance of the thalweg bedform in flow resistance generation in these stream types.

The inspection of residuals can be helpful in understanding underlying processes contributing to flow resistance as well as identifying potential grouping and generalizations. An examination of student residuals of the *f* versus h/σ_z 50% channel width regression (Figure 7) indicates that h/σ_z overpredicts resistance in the steeper cascade reaches as well as the plane-bed reach. The plane-bed reach measurements were also consistently overpredicted, especially at bankfull flow. In contrast, the transitional reach measurements were predicted relatively well; the slightly greater bedforms expressed in the transitional reach translate to more appropriate use of h/σ_z for flow resistance prediction. In general, the step pool reach predictions were least biased, although underprediction of flow resistance using h/σ_z is apparent at times, especially for lower-magnitude discharges. More substantial overprediction of flow resistance was noted for the steepest cascade channels (FC-5 and 6) at the highest flow; flow characteristics may be shifting toward a skimming regime at bankfull flow. In a full skimming regime, hydraulic jumps and aeration are eliminated and the flow becomes completely critical or supercritical [*Comiti et al*., 2009], instead of alternating between supercritical and subcritical flow in the nappe regime typical in these stream reaches. With reach-average Froude numbers of about 0.50 and only partial submergence of the bedforms, a full skimming regime is not occurring; however, these steep, higher-flow measurements may have been collected in a transition zone. *Comiti et al*. [2009] found a sharp reduction in flow resistance in their mobile-bed laboratory study with a critical flow

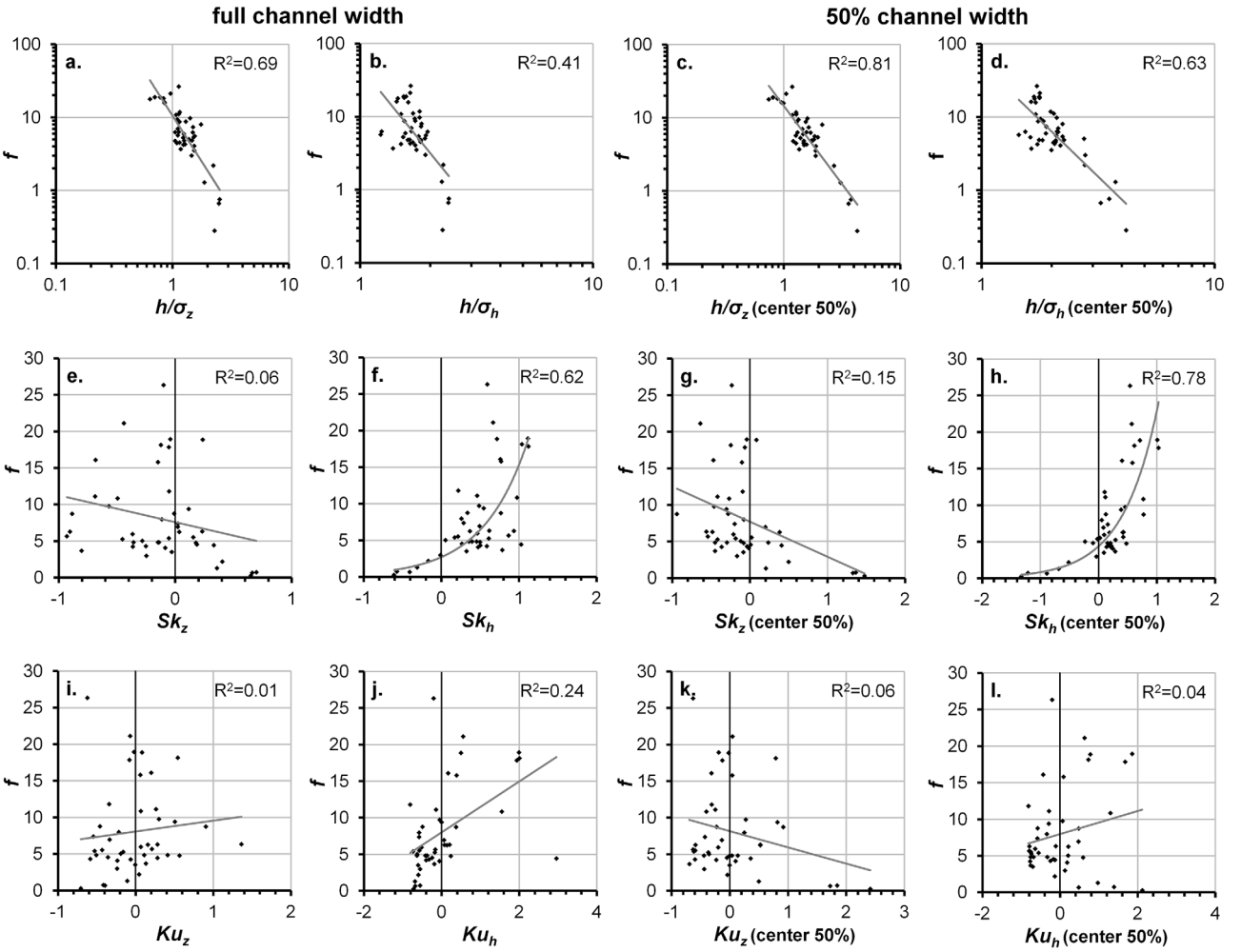

Figure 5. Relationship of Darcy-Weisbach *f* with standard deviation (σ), skew (*Sk*) and kurtosis (*Ku*) of detrended bed elevations (z) and depths (h), for the entire channel width and the center 50% of the width.

depth/average step height (h_c/z) ratio of 1.2 to 1.7, while bankfull flows in FC-5 and FC-6 have h_c/z ratios of about 1.1 and 1.0, respectively.

While Sk_z is poorly correlated with flow resistance (Figures 5e and 5g), Sk_h does correlate well with flow resistance (Figures 5f and 5h), with flow resistance increasing as Sk_h increases. Mechanistically, this finding makes sense because increasing positive skew indicates outlying higher magnitude depths are present (Figure 2), providing more opportunity for both form and spill resistance. As with relative bedform submergence, *Sk* predicted using only the center 50% of the channel width correlates better with flow resistance ($R^2 = 0.78$) than using the entire channel width ($R^2 = 0.62$). Sk_h adjusted to maintain a positive value (to allow a power model fit) was combined with h/σ_z in a multiple regression model. The resulting model explained 83% of the flow resistance variation, with both variables being highly significant (0.00048 and 0.0058, respectively). Sk_h and h/σ_z were not well correlated with eachother ($R^2 = 0.25$).

For the Fraser channels, Ku_z and Ku_h correlate poorly with flow resistance (Figures 5i–5l). This data set indicates that *Ku* does not have value for predicting flow resistance in high-gradient channels.

4.2. *Sk-Ku* Plane

Sk versus *Ku* plots of the Fraser data indicate substantially different results when comparing analyses performed with the entire channel width versus the center 50% of the channel width (Figure 6). Plots also varied between detrended bed elevations and depth. In general, the plane bed measurements are grouped

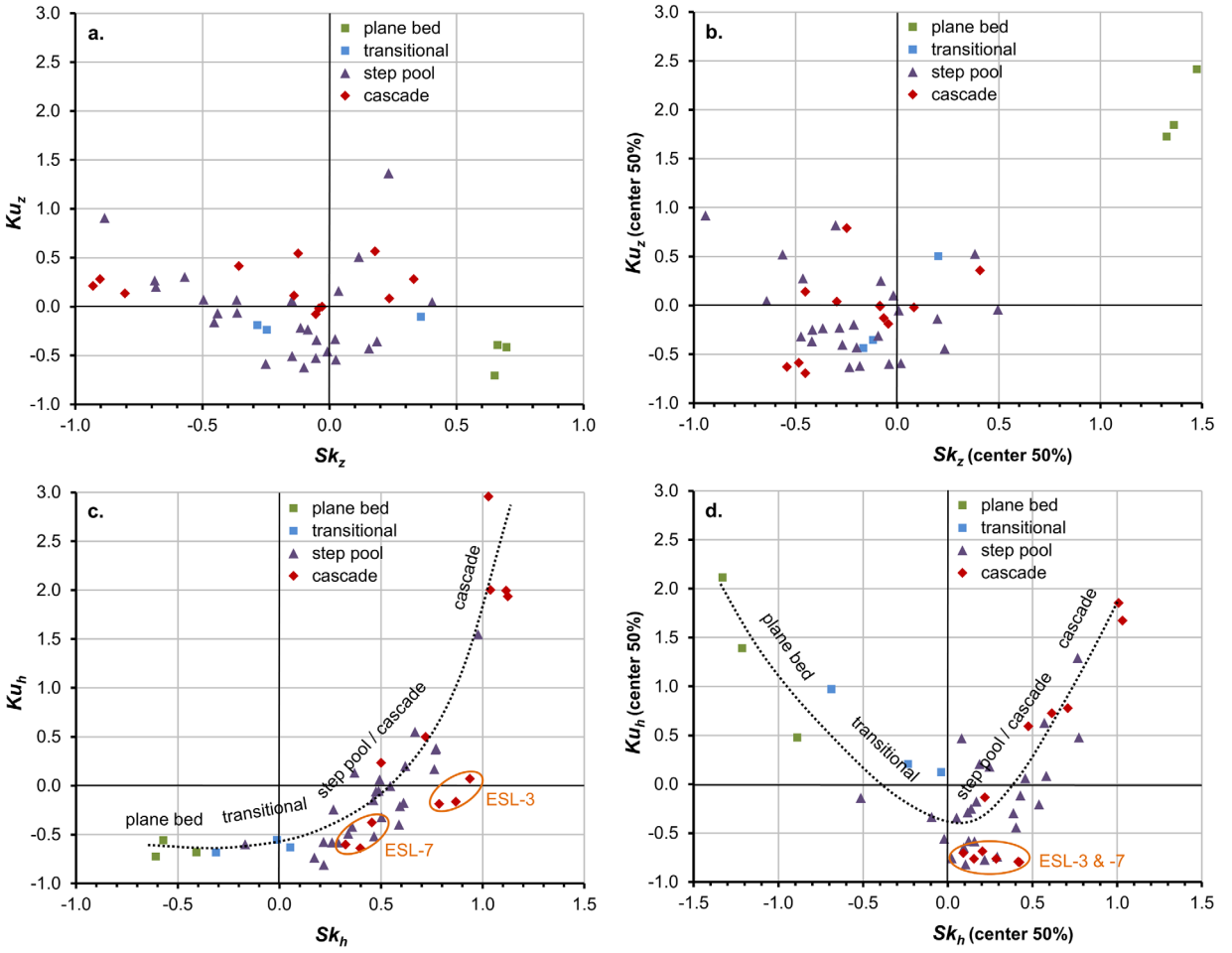

Figure 6. *Sk* – *Ku* plane, for both (a, b) detrended elevations (*z*) and (c, d) depths (*h*), for the entire channel width and the center 50% of the width.

differently than measurements collected in channels with more substantial bedforms, and cascade channels have higher Ku_z values than step pool channels.

For the Fraser database, the plane bed measurements (Figure 6b) match the findings of *Coleman et al.* [2011] (Figure 8) for laboratory-based armored gravel and sand plane bed channels. In these cases, plane bed channels are shown to have both large positive Sk_z and large positive Ku_z. However, this is only the case when the outer 50% of the channel beds are excluded. Ku_z is sensitive to these bank effects, with the plane bed Ku_z becoming negative when the channel edges are included in the data set (Figure 6a). Sk_z values are also impacted by bank effects, but not as substantially. Additionally, the cascade and step pool values for Ku_z versus Sk_z plot similarly to the results found by the grouping of ripple and dune sand bed channels; channels with bedforms tend to have negative to slightly positive Sk_z values, with *Ku* ranging from -1 to $+1$. Hence, the Fraser data set generally supports the summary presented in *Coleman et al.* [2011, Figure 9], with bedform channels grouped in the vicinity of the origin and plane bed channels grouped independently with both positive Sk_z and Ku_z. Importantly, the Fraser data set indicates that bank effects need to be excluded for this generalization to hold.

Variation between stream channel types is evident in the *Sk* versus *Ku* plots (Figures 6c and 6d), although these relationships vary between the full channel width and 50% channel width data sets. This variation is expressed as a spectrum, with the channels with the most cascade-like features having the highest Ku_h and Sk_h values and those with more of a cascade to step pool transitional form (ESL-3 and 7) being grouped with values collected in step pool channels. On the negative Sk_h side of the plots, this spectrum is also

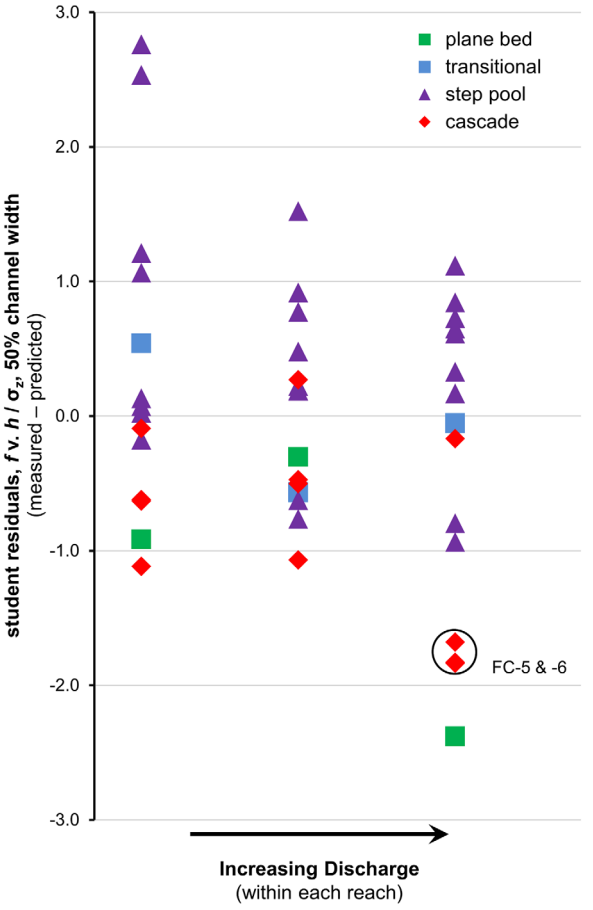

Figure 7. Student residuals of f v. h/σ_z regression (50% channel width).

evident in the plane bed to step pool transitional reaches, with the least bedforms associated with most negative Sk_h. With the plane bed (and transitional) Ku_h values being most sensitive to bank effects, the variation relationship shifts most substantially in channels with the least bedforms, while the relationships are similar for channels with greater bedforms.

4.3. Full Versus 50% Channel Width

Exclusion of the channel bank zone in these narrow streams has substantial impacts upon computations, for both the flow resistance and the *Sk-Ku* plane evaluations. For example, including only the center 50% of the channel width about the thalweg increases the explained variance of f (using h/σ_z) from 69 to 81%. Bed variability due to clasts and wood on the outer edges of the channels provide less contribution to average reach flow resistance than bed variability in the vicinity of the thalweg. This finding complements field observations that velocity (and unit discharge) is substantially higher in the vicinity of the thalweg than toward the channel edges; edge effects are substantial in these high-gradient Fraser stream reaches. As with relative bedform submergence, skew as predicted using only the center 50% of the channel width explains more variability in f ($R^2 = 0.78$ versus 0.62), providing additional evidence that bed variability in the vicinity of the thalweg contributes substantially more to flow resistance than the channel edges. Additionally, the results of the *Sk – Ku* analyses match previous research [*Coleman et al*., 2011] only if the bank zones are excluded from the analyses. Hence, in these relatively small high-gradient streams, the channel in the vicinity of the thalweg is more effective and most appropriate in random field analyses.

4.4. Elevation Versus Depth Fields

Past research on random fields of stream channels has focused on elevation variability [*Furbish*, 1987; *Robert*, 1988; *Clifford et al*., 1992; *Nikora et al*., 1997; *Nikora et al*., 1998; *Aberle and Smart*, 2003; *Smart et al*., 2004; *Aberle and Nikora*, 2006; *Aberle et al*., 2010; *Coleman et al*., 2011]; however, these findings indicate that depth fields can also be valuable in high-gradient streams. Histograms (Figure 4) illustrate that, in lower gradient channels, depth variability appears to be similar to the mirror of bed elevation variability, due to a relatively planar water surface. As stream gradient increases, flow becomes more varied and the variables (elevation and depth) diverge. This mirroring is evident in the histograms for FC-2 and ESL-3. The σ and Sk values can quantify this effect (Figure 4 and Appendix A). In lower-gradient reaches (ESl-6 and 7, FC1 and 2), σ_z and σ_h are very similar, while in higher-gradient reaches (ESL-5, FC-4, 5, and 6), σ_z and σ_h are substantially different. For Sk, the same lower-gradient reaches show similar magnitudes but opposite signs and are also more divergent as gradient increases, with Sk_z and Sk_h both positive for the steepest reaches, FC-5 and 6. As indicated by σ, the variables diverge above slopes of about 9% (Figure 8).

With relative bedform submergence (h/σ_z) inversely proportional to flow resistance in the Fraser stream reaches (Figures 5a–5d), submergence based on σ_z is more effective than σ_h for prediction ($R^2 = 0.81$ versus

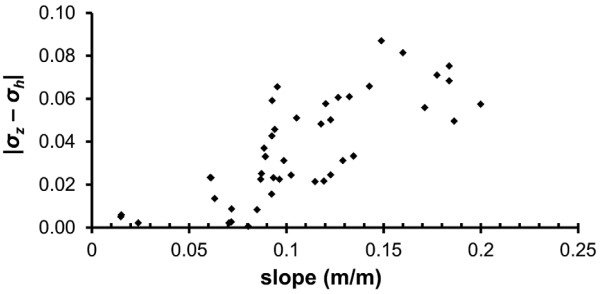

Figure 8. Divergence of σ_z and σ_h by channel slope.

0.63). However, while Sk_z does not correlate well with flow resistance (Figures 5e and 5g), Sk_h does correlate well (Figures 5f and 5h). Sk_h having more explanatory power than Sk_z apparently relates to the divergence of *z* and *h* as stream gradient increases and flow becomes more varied, with rapidly varied flow of alternating supercritical and subcritical flow on the subreach scale as slope increases. In the Ku_h – Sk_h plots (Figures 6c and 6d), the mirror effect of *h* versus *z* is also evident, with opposite signed *Sk* values for the lower-gradient plane bed and transitional measurements. The differences between detrended *z* and *h* plots for the higher-gradient channels, with *h* showing more consistent variation by channel type, illustrate the usefulness of depth fields. Random field computations based on both elevation and depth have value for predicting flow resistance and sorting stream types in these Fraser stream channels.

4.5. Random Field Analysis and Geomorphic Characterization

The illustrated field plots (Figure 4) indicate several interesting geomorphic characteristics, with analysis ramifications. For example, cascade reach ESL-3 is overly wide, with a substantial amount of less-effective flow area on the left (west) side of the channel and a bar in the middle of the channel. This is quantified by the substantially negative elevation skew, with the largest negative magnitude skews in the Fraser database. This is mirrored by the large magnitude positive depth skew. Channels with excessively negative elevation skews may be directly analogous to high width/depth ratio channels. When only the center 50% of the channel width is accounted for, the skew magnitude decreases and is no longer atypical. Additionally, when only the center 50% of the channel is taken into account, *h* substantially increases and σ_z increases to a lesser extent, resulting in a higher h/σ_z that better reflects the measured flow resistance. This more active right portion of the channel has more step-pool characteristics than the left channel; hence, this reach may be more appropriately characterized as having a step-pool-dominated bedform, explaining the outlying *Sk-Ku* plot position (Figures 6c and 6d). In contrast, the depth variability plot for FC-5 indicates a bedform that is dominated by a relatively random pattern, with long stretches of continuously tumbling flow over and around clasts and wood. A couple of steps are noted, but extend for a small minority of the channel length. Unlike reach ESL-3, this reach is fairly clearly a cascade channel as defined by *Montgomery and Buffington* [1997]. Similarly, the depth variability plot for ESL-4 shows a number of channel-spanning steps that are formed by bedrock, clasts, and wood; this is clearly a step-pool-dominated channel. Reach ESL-1 (Figures 1 and 3) also has a dominant step-pool channel form.

4.6. Data Set Limitations

The data set has high resolution for above the low-flow water surface, but has a lower resolution in the deeper portions of the channels where the gridded total station data were used to fill gaps in the LiDAR data set. While many points were collected, the DEMs were necessarily interpolated to the 5 cm resolution in these wetted low flow areas. Additionally, since the water surface DEM was developed using thalweg and left/right edge of banks, as opposed to using a more comprehensive method such as oblique LiDAR scanning, there is error incorporated into the depth estimates. This is especially the case where the water surface substantially varies across the width of a section. LiDAR scanning of the water surface was not possible due to the time required to perform the scanning and excessively challenging field conditions during high flow. These data collection limitations may introduce error in the results.

5. Conclusions

A high-gradient stream channel data set, with measured average reach velocity and flow resistance measurements and LiDAR-derived characterization of flow resistance elements, provided an opportunity to explore three-dimensional spatial relationships in cascade, step pool and plane bed stream channels. Random field variables, such as the mean, variance, skew, and kurtosis statistical moments, were explored for

their utility in quantifying bedforms and their contribution to flow resistance. In general, h/σ was found to be highly related to flow resistance, Sk_h is well related to flow resistance while Sk_z is not, and *Ku* is poorly correlated with flow resistance in these high-gradient channels. *Sk* versus *Ku* plots were developed for the detrended elevation and depth, for both the full and 50% channel widths. The depth *Sk-Ku* field plots indicate a spectrum of channel types across the plane, from plane bed to cascade. While this data set indicates that flow resistance prediction using relative bedform submergence computed from the three-dimensional variability is powerful for prediction, it provides no advantage to submergence computed from simpler-to-measure longitudinal profiles. Exclusion of the channel bank zone in these narrow streams has substantial impacts upon computations, for both the flow resistance and the *Sk-Ku* plane evaluations. Bed variability due to clasts and wood on the outer edges of the channels provide less contribution to average reach flow resistance than bed variability in the vicinity of the thalweg; the more effective portion of the channel in the vicinity of the thalweg, with higher flow conveyance, can be most appropriate in random field analyses.

Appendix A

Table A1. Spatial Characterization Data Set Implemented in Analyses

								Full Channel Width									
ID	Channel Type	Date	f	V (m/s)	Q (m^3/s)	L (m)	S (m/m)	n	h (m)	σ_z (m)	h/σ_z	Sk_z	Ku_z	σ_h (m)	h/σ_h	Sk_h	Ku_h
ESL1	step-pool	10/06/2008	4.5	0.65	0.56	29.4	0.095	32288	0.31	0.27	1.15	0.19	−0.36	0.17	1.82	0.27	−0.24
ESL1	step-pool	22/07/2008	9.4	0.42	0.24	27.3	0.105	30100	0.24	0.22	1.10	0.12	0.51	0.14	1.71	0.55	−0.0053
ESL2	step-pool	09/07/2007	7.0	0.45	0.22	13.9	0.093	16346	0.21	0.19	1.11	0.022	−0.33	0.13	1.66	0.49	0.061
ESL2	step-pool	06/06/2008	4.8	0.61	0.53	13.7	0.094	17565	0.27	0.19	1.40	−0.15	−0.51	0.15	1.81	0.36	−0.42
ESL2	step-pool	15/07/2008	4.3	0.59	0.31	14.0	0.093	14862	0.22	0.17	1.29	−0.25	−0.59	0.14	1.64	0.50	−0.32
ESL3	cascade	10/07/2007	6.3	0.49	0.22	10.7	0.123	17839	0.16	0.16	1.06	−0.90	0.28	0.13	1.24	0.94	0.07
ESL3	cascade	07/06/2008	3.7	0.71	0.46	10.2	0.129	18427	0.19	0.16	1.18	−0.80	0.13	0.14	1.38	0.79	−0.19
ESL3	cascade	15/07/2008	5.7	0.54	0.30	10.7	0.119	17216	0.18	0.16	1.11	−0.93	0.21	0.15	1.22	0.87	−0.17
ESL4	step-pool	10/07/2007	8.7	0.45	0.21	15.8	0.123	15517	0.21	0.18	1.15	−0.89	0.91	0.13	1.55	0.77	0.37
ESL4	step-pool	07/06/2008	6.3	0.63	0.61	15.6	0.120	17338	0.29	0.26	1.13	0.23	1.36	0.18	1.66	0.62	0.20
ESL4	step-pool	14/07/2008	9.7	0.50	0.32	15.9	0.118	14620	0.28	0.19	1.42	−0.57	0.30	0.15	1.80	0.49	−0.053
ESL5	step-pool	12/07/2007	16.1	0.36	0.19	13.5	0.149	17212	0.17	0.19	0.86	−0.68	0.20	0.12	1.44	0.76	0.17
ESL5	step-pool	09/06/2008	11.1	0.52	0.50	12.5	0.160	17924	0.23	0.20	1.14	−0.69	0.26	0.14	1.69	0.46	−0.15
ESL5	step-pool	14/07/2008	10.8	0.48	0.33	13.9	0.143	17334	0.21	0.19	1.08	−0.50	0.069	0.14	1.50	0.98	1.55
ESL6	plane-bed	13/07/2007	0.67	0.58	0.19	6.5	0.015	7052	0.17	0.069	2.50	0.66	−0.39	0.073	2.39	−0.41	−0.68
ESL6	plane-bed	09/06/2008	0.28	1.32	0.52	6.4	0.024	7559	0.25	0.11	2.30	0.65	−0.71	0.11	2.26	−0.61	−0.73
ESL6	plane-bed	14/07/2008	0.76	0.61	0.32	6.4	0.015	6454	0.24	0.093	2.55	0.70	−0.42	0.10	2.41	−0.57	−0.56
ESL7	cascade	12/07/2007	4.8	0.50	0.20	22.9	0.087	22774	0.17	0.13	1.26	−0.36	0.41	0.11	1.60	0.40	−0.64
ESL7	cascade	08/06/2008	3.5	0.69	0.52	22.1	0.085	24188	0.24	0.16	1.54	−0.03	−0.0030	0.14	1.74	0.33	−0.60
ESL7	cascade	15/07/2008	4.8	0.55	0.30	24.0	0.081	20965	0.22	0.15	1.48	−0.14	0.11	0.13	1.63	0.46	−0.38
ESL8	Step-pool	11/07/2007	6.0	0.46	0.21	31.4	0.089	26234	0.18	0.14	1.26	−0.36	0.068	0.11	1.56	0.47	−0.52
ESL8	step-pool	09/06/2008	4.2	0.64	0.46	30.7	0.094	34626	0.21	0.17	1.24	−0.36	−0.064	0.14	1.50	0.59	−0.40
ESL8	step-pool	16/07/2008	5.3	0.53	0.29	32.6	0.087	29620	0.20	0.16	1.24	−0.45	−0.16	0.13	1.53	0.61	−0.18
ESL9	step-pool	11/07/2007	8.8	0.43	0.20	16.2	0.103	16313	0.21	0.16	1.30	−0.0080	−0.46	0.12	1.72	0.34	−0.49
ESL9	step-pool	08/06/2008	5.5	0.64	0.57	16.3	0.115	17392	0.29	0.19	1.56	0.16	−0.43	0.15	1.91	0.22	−0.58
ESL9	step-pool	16/07/2008	7.4	0.47	0.28	16.5	0.097	15057	0.25	0.17	1.50	0.026	−0.54	0.14	1.82	0.29	−0.58
FC1	transitional	05/07/2007	3.0	0.40	0.049	23.7	0.061	14403	0.11	0.074	1.46	−0.25	−0.24	0.057	1.90	−0.01	−0.56
FC1	transitional	11/06/2008	1.3	0.79	0.23	23.1	0.063	16142	0.18	0.10	1.88	0.36	−0.11	0.082	2.24	−0.31	−0.69
FC1	transitional	23/07/2008	5.0	0.30	0.037	23.2	0.061	13613	0.10	0.072	1.38	−0.28	−0.19	0.053	1.90	0.055	−0.63
FC2	step-pool	07/07/2007	4.1	0.37	0.043	15.1	0.072	7041	0.10	0.068	1.54	−0.085	−0.23	0.061	1.72	0.48	−0.060
FC2	step-pool	11/06/2008	2.2	0.66	0.24	14.4	0.071	7558	0.21	0.095	2.24	0.40	0.045	0.093	2.28	−0.17	−0.60
FC2	step-pool	23/07/2008	8.0	0.28	0.038	14.2	0.072	6523	0.12	0.070	1.76	−0.11	−0.22	0.067	1.83	0.26	−0.58
FC3	step-pool	06/07/2007	11.8	0.26	0.045	14.9	0.089	6920	0.12	0.11	1.16	−0.051	−0.34	0.068	1.80	0.22	−0.81
FC3	step-pool	12/06/2008	5.4	0.51	0.22	13.5	0.092	8155	0.22	0.14	1.53	−0.053	−0.53	0.12	1.78	0.17	−0.74
FC3	step-pool	22/07/2008	26.3	0.18	0.039	12.2	0.099	6741	0.12	0.10	1.13	−0.10	−0.62	0.070	1.65	0.59	−0.21
FC4	step-pool	07/07/2007	21.1	0.24	0.042	19.0	0.132	8951	0.14	0.14	0.96	−0.44	−0.068	0.083	1.64	0.67	0.55
FC4	step-pool	12/06/2008	6.3	0.59	0.22	18.9	0.135	8916	0.25	0.17	1.49	0.036	0.16	0.13	1.95	0.37	0.13
FC4	step-pool	21/07/2008	15.8	0.27	0.045	19.8	0.127	9154	0.13	0.15	0.85	−0.15	0.062	0.078	1.61	0.77	0.38
FC5	cascade	08/07/2007	18.2	0.24	0.015	13.1	0.171	4281	0.09	0.11	0.84	−0.12	0.54	0.060	1.54	1.04	2.00
FC5	cascade	25/06/2008	4.5	0.64	0.15	11.9	0.186	5198	0.16	0.14	1.09	0.33	0.28	0.094	1.68	1.03	2.96
FC5	cascade	17/07/2008	18.9	0.24	0.017	11.9	0.184	3880	0.10	0.12	0.78	0.24	0.082	0.062	1.57	0.72	0.50
FC6	cascade	08/07/2007	17.8	0.24	0.014	19.8	0.184	6596	0.08	0.13	0.64	−0.053	−0.079	0.058	1.45	1.12	1.93
FC6	cascade	25/06/2008	4.8	0.62	0.14	19.1	0.200	7308	0.14	0.14	1.06	0.18	0.56	0.079	1.82	0.50	0.23
FC6	cascade	17/07/2008	18.9	0.23	0.017	20.6	0.178	5996	0.09	0.13	0.71	−0.041	−0.020	0.059	1.54	1.12	1.99

				50% Channel Width									
ID	Channel Type	Date	Q (m^3/s)	n	h (m)	σ_z (m)	h/σ_z	Sk_z	Ku_z	σ_h (m)	h/σ_h	Sk_h	Ku_h
ESL1	step-pool	22/07/2008	0.24	13833	0.27	0.20	1.34	−0.30	0.82	0.15	1.79	0.39	−0.30
ESL2	step-pool	09/07/2007	0.22	7020	0.27	0.18	1.45	0.20	−0.14	0.12	2.13	0.08	0.47
ESL2	step-pool	06/06/2008	0.53	7541	0.34	0.20	1.73	0.23	−0.45	0.15	2.26	−0.10	−0.34
ESL2	step-pool	15/07/2008	0.31	6463	0.28	0.18	1.57	−0.04	−0.60	0.14	2.06	0.14	−0.25
ESL3	cascade	10/07/2007	0.22	7953	0.22	0.17	1.32	−0.48	−0.59	0.14	1.54	0.42	−0.79
ESL3	cascade	07/06/2008	0.46	8161	0.25	0.18	1.36	−0.45	−0.70	0.15	1.64	0.29	−0.76
ESL3	cascade	15/07/2008	0.30	8072	0.23	0.18	1.27	−0.54	−0.63	0.16	1.44	0.42	−0.80
ESL4	step-pool	10/07/2007	0.21	7087	0.24	0.19	1.29	−0.94	0.92	0.14	1.75	0.77	0.48
ESL4	step-pool	07/06/2008	0.61	7880	0.36	0.23	1.57	−0.56	0.52	0.17	2.11	0.43	−0.12
ESL4	step-pool	14/07/2008	0.32	7015	0.32	0.20	1.60	−0.46	0.27	0.15	2.10	0.46	0.059
ESL5	step-pool	12/07/2007	0.19	7753	0.20	0.21	0.96	−0.47	−0.32	0.12	1.63	0.40	−0.44
ESL5	step-pool	09/06/2008	0.50	8001	0.28	0.22	1.28	−0.42	−0.25	0.14	2.04	0.12	−0.29
ESL5	step-pool	14/07/2008	0.33	8152	0.26	0.22	1.19	−0.27	−0.40	0.15	1.71	0.77	1.29
ESL6	plane-bed	13/07/2007	0.19	3308	0.20	0.055	3.60	1.33	1.72	0.061	3.25	−0.89	0.47
ESL6	plane-bed	09/06/2008	0.52	3416	0.31	0.072	4.29	1.47	2.41	0.074	4.17	−1.33	2.11
ESL6	plane-bed	14/07/2008	0.32	3051	0.28	0.073	3.78	1.36	1.84	0.078	3.53	−1.21	1.39
ESL7	cascade	12/07/2007	0.20	11144	0.20	0.13	1.49	−0.45	0.14	0.11	1.83	0.16	−0.76
ESL7	cascade	08/06/2008	0.52	11306	0.28	0.15	1.88	−0.08	−0.0040	0.14	1.99	0.092	−0.71
ESL7	cascade	15/07/2008	0.30	10523	0.26	0.15	1.76	−0.30	0.036	0.14	1.77	0.21	−0.69
ESL8	step-pool	11/07/2007	0.21	12162	0.22	0.15	1.47	−0.21	−0.20	0.11	1.89	0.095	−0.65
ESL8	step-pool	09/06/2008	0.46	16053	0.25	0.17	1.49	−0.37	−0.23	0.14	1.74	0.22	−0.77
ESL8	step-pool	16/07/2008	0.29	13374	0.22	0.16	1.39	−0.42	−0.37	0.14	1.62	0.29	−0.74
ESL9	step-pool	11/07/2007	0.20	7399	0.24	0.15	1.55	−0.28	−0.23	0.13	1.84	0.12	−0.58
ESL9	step-pool	08/06/2008	0.57	8048	0.33	0.18	1.84	0.019	−0.59	0.16	2.09	0.023	−0.76
ESL9	step-pool	16/07/2008	0.28	7151	0.27	0.16	1.63	−0.20	−0.43	0.14	1.89	0.16	−0.59
FC1	transitional	05/07/2007	0.049	7193	0.13	0.071	1.88	−0.17	−0.44	0.048	2.79	−0.037	0.12
FC1	transitional	11/06/2008	0.23	8062	0.23	0.074	3.07	0.20	0.50	0.061	3.76	−0.69	0.97
FC1	transitional	23/07/2008	0.037	6716	0.12	0.068	1.82	−0.12	−0.36	0.045	2.75	−0.23	0.20
FC2	step-pool	07/07/2007	0.043	3638	0.12	0.066	1.89	−0.018	0.10	0.057	2.18	0.25	0.18
FC2	step-pool	11/06/2008	0.24	3799	0.25	0.091	2.71	0.50	−0.04	0.089	2.77	−0.51	−0.14
FC2	step-pool	23/07/2008	0.038	3169	0.14	0.068	2.14	−0.081	0.25	0.065	2.22	0.052	−0.34
FC3	step-pool	06/07/2007	0.045	3649	0.13	0.10	1.28	−0.093	−0.31	0.067	1.98	0.11	−0.82
FC3	step-pool	12/06/2008	0.22	4226	0.26	0.13	1.96	−0.18	−0.62	0.12	2.23	−0.021	−0.56
FC3	step-pool	22/07/2008	0.039	2990	0.12	0.10	1.19	−0.24	−0.63	0.069	1.73	0.54	−0.21
FC4	step-pool	07/07/2007	0.042	4196	0.16	0.15	1.05	−0.64	0.046	0.088	1.78	0.57	0.63
FC4	step-pool	12/06/2008	0.22	4285	0.28	0.16	1.70	0.38	0.52	0.13	2.13	0.19	0.21
FC4	step-pool	21/07/2008	0.045	4456	0.15	0.15	1.00	−0.11	0.04	0.085	1.71	0.58	0.084
FC5	cascade	08/07/2007	0.015	2087	0.10	0.11	0.89	−0.25	0.79	0.055	1.78	0.62	0.72
FC5	cascade	25/06/2008	0.15	2557	0.17	0.13	1.28	0.41	0.36	0.083	2.03	0.22	−0.14
FC5	cascade	17/07/2008	0.017	1838	0.11	0.13	0.81	0.083	−0.022	0.063	1.68	0.71	0.78
FC6	cascade	25/06/2008	0.14	3563	0.16	0.14	1.20	−0.083	−0.011	0.079	2.08	0.48	0.59
FC6	cascade	17/07/2008	0.017	2898	0.11	0.13	0.81	−0.043	−0.19	0.060	1.77	1.01	1.85

Acknowledgments

Appreciation is expressed to the National Science Foundation for funding (grant EAR0608918), to the U. S. Department of Agriculture (USDA) Natural Resources Conservation Service for additional funding, to the USDA Forest Service Rocky Mountain Research Station for hosting the research on the Fraser Experimental Forest, and to our field assistants Mark Hussey, Dan Dolan, and Lina Polvi. Appreciation is also expressed for helpful comments on portions of this and related manuscripts by Sara Rathburn, Chester Watson, Roman Weichert, Andre Zimmermann, and an anonymous reviewer.

References

Aberle, J., and V. Nikora (2006), Statistical properties of armored gravel bed surfaces, *Water Resour. Res.*, *42*, W11414, doi:10.1029/2005WR004674.

Aberle, J., and G. M. Smart (2003), The influence of roughness structure on flow resistance on steep slopes, *J. Hydraul. Res.*, *41*(3), 259–269, doi:10.1080/00221680309499971.

Aberle, J., V. Nikora, M. Henning, B. Ettmer, and B. Hentschel (2010), Statistical characterization of bed roughness due to bedforms: A field study in the Elbe River at Aken, Germany, *Water Resour. Res.*, *46*, W03521, doi:10.1029/2008WR007406.

Ataman, E., V. K. Aatre, and K. M. Wong (1981), Some statistical properties of median filters, *IEEE Trans. Acoust. Speech Signal Process.*, *29*(5), 1073–1075.

Clifford, N. J., A. Robert, and K. S. Richards (1992), Estimation of flow resistance in gravel-bedded rivers: A physical explanation of the multiplier of roughness length, *Earth Surf. Processes Landforms*, *17*, 111–126, doi:10.1002/esp.3290170202.

Coleman, S. E., V. I. Nikora, and J. Aberle (2011), Interpretation of alluvial beds through bed-elevation distribution moments, *Water Resour. Res.*, *47*, W11505, doi:10.1029/2011WR010672.

Comiti F., D. Cadol, and E. Wohl (2009), Flow regimes, bed morphology, and flow resistance in self-formed step-pool channels, *Water Resour. Res.*, *45*, W04424, doi:10.1029/2008WR007259.

Curran, J. H., and E. E. Wohl (2003), Large woody debris and flow resistance in step-pool channels, Cascade Range, Washington, *Geomorphology*, *51*(1-3), 141–157.

David, G. C. L., E. Wohl, S. E. Yochum, and B. P. Bledsoe (2010a), Controls on spatial variations in flow resistance along steep mountain streams, *Water Resour. Res.*, *46*, W03513, doi:10.1029/2009WR008134.

David, G. C. L., E. Wohl, S. E. Yochum, and B. P. Bledsoe (2010b), Controls on at-a-station hydraulic geometry in steep headwater streams, Colorado, USA. *Earth Surf. Processes Landforms*, doi:10.1002/esp.2023.

David, G. C. L., E. Wohl, S. E. Yochum, and B. P. Bledsoe (2011), Comparative analysis of bed resistance partitioning in high gradient streams, *Water Resour. Res.*, *47*, W07507, doi:10.1029/2010WR009540.
Ferguson, R. (2007), Flow resistance equations for gravel- and boulder-bed streams, *Water Resour. Res.*, *43*, W05427, doi:10.1029/2006WR005422.
Furbish, D. J. (1987), Conditions for geometric similarity of coarse-bed roughness, *Math. Geol.*, *4*(19), doi:10.1007/BF00897840.
Gallagher, N. C., and G. L. Wise (1981), A theoretical analysis of the properties of median filters, *IEEE Trans. Acoust. Speech Signal Process.*, *29*(6), 1136–1141.
Hino, M. (1968), Equilibrium-range spectra of sand waves formed by flowing water, *J. Fluid Mech.*, *34*(3), 565–273, doi:10.1017/S0022112068002089.
Jain, S. C., and J. F. Kennedy (1974), The spectral evolution of sedimentary bedforms, *J. Fluid Mech.*, *63*(2) 301–314, doi:10.1017/S0022112074001157.
Kaufmann, P. R. (1987), Channel morphology and hydraulic characteristics of torrent-impacted forest streams in the Oregon Coast Range, USA, PhD dissertation, Oreg. State Univ., Corvallis.
Kaufmann, P. R., J. M. Faustini, D. P. Larsen, and M. A. Shirazi (2008), A roughness-corrected index of relative bed stability for regional stream surveys, *Geomorphology*, *99*, 150–170.
Kennedy, J. F. (1963), The mechanics of dunes and antidunes in erodible-bed channels, *J. Fluid Mech.*, *16*(4), 521–544, doi:10.1017/S0022112063000975.
Lee, A. J., and R. I. Ferguson (2002), Velocity and flow resistance in step-pool streams, *Geomorphology*, *46*, 59–71.
MacFarlane, W. A., and E. Wohl (2003), Influence of step composition on step geometry and flow resistance in step-pool streams of the Washington Cascades, *Water Resour. Res.*, *39*(2), 1037, doi:10.1029/2001WR001238.
Nikora, V., and J. Walsh (2004), Water-worked gravel surfaces: Higher-order structure functions at the particle scale, *Water Resour. Res.*, *40*, W12601, doi:10.1029/2004WR003346.
Nikora, V. I., D. G. Goring, and B. J. F. Biggs (1998), On gravel-bed roughness characterization, *Water Resour. Res.*, *34*(3), 517–527, doi:10.1029/97WR02886.
Nikora, V. I., A. N. Sukhodolov, and P. M. Rowinski (1997), Statistical sand wave dynamics in one-directional water flows, *J. Fluid Mech.*, *351*, 17–39, doi:10.1017/S0022112097006708.
Nitsche, M., D. Rickenmann, J. W. Kirchner, J. M. Turowski, and A. Badoux (2012), Macroroughness and variations in reach-averaged flow resistance in steep mountain streams, *Water Resour. Res.*, *48*, W12518, doi:10.1029/2012WR012091.
Nordin, C. J. (1971), Statistical properties of dune profiles, *U. S. Geol. Surv. Prof. Pap.*, *562-F*.
Reid, D. E., and E. J. Hickin (2008), Flow resistance in steep mountain streams, *Earth Surf. Processes Landforms*, *33*, 2211–2240.
Robert, A. (1988), Statistical properties of sediment bed profiles in alluvial channels, *Math. Geol.*, *20*(3), 205–225, doi:10.1007/BF00890254.
Smart, G., J. Aberle, M. Duncan, and J. Walsh (2004), Measurement and analysis of alluvial bed roughness, *J. Hydraul. Res.*, *43*(3), 227–237.
Trevisani, S., M. Cavalli, and L. Marchi (2010), Reading the bed morphology of a mountain stream: A geomorphometric study on high-resolution topographic data, *Hydrol. Earth Syst. Sci.*, *14*, 393–405.
Tukey, J. W. (1974), Nonlinear (nonsuperposable) methods for smoothing data, *IEEE Electron. Aerosp. Syst. Conv.*, *673*.
Walden, M. G. (2004), Estimation of average stream velocity, *J. Hydraul. Eng.*, *130*(11), 1119–1122.
Wilcox, A. C., J. M. Nelson, and E. E. Wohl (2006), Flow resistance dynamics in step-pool stream channels: 2. partitioning between grain, spill and woody debris resistance, *Water Resour. Res.*, *42*, W05419, doi:10.1029/2005WR004278.
Wohl, E., and D. M. Merritt (2008), Reach-scale channel geometry of mountain streams, *Geomorphology*, *93*, 168–185.
Yochum, S., and B. Bledsoe (2010), Flow resistance estimation in high-gradient streams, paper presented at 4th Federal Interagency Hydrologic Modeling Conference, Las Vegas, Nev., 27 Jun-1 Jul. [Available at: http://acwi.gov/sos/conf/JFIC2010-1st-Announcement-111909-jmb-wTOC.pdf.]
Yochum, S. E. (2010), Flow resistance prediction in high-gradient streams, PhD dissertation, Colo. State Univ., Fort Collins.
Yochum, S. E., B. P. Bledsoe, G. C. L. David, and E. Wohl (2012), Velocity prediction in high-gradient channels, *J. Hydrol.*, *424-425*, 84–98, doi:10.1016/j.jhydrol.2011.12.031.
Yochum, S. E., F. Comiti, E. Wohl, G. C. L. David, and L. Mao (2014), Photographic guidance for selecting flow resistance coefficients in high-gradient channels, *Gen. Tech. Rep. RMRS-GTR-323*, 91 p., U. S. Dep. of Agric., For. Serv., Rocky Mt. Res. Stn., Fort Collins, Colo.
Zimmermann, A. (2010), Flow resistance in steep streams: An experimental study, *Water Resour. Res.*, *46*, W09536, doi:10.1029/2009WR007913.